Bull Earthquake Eng (2012) 10:135–159
DOI 10.1007/s10518-010-9209-3

ORIGINAL RESEARCH PAPER

Experimental testing, numerical modelling and seismic strengthening of traditional stone masonry: comprehensive study of a real Azorian pier

Alexandre A. Costa · António Arêde · Aníbal Costa · João Guedes · Bruno Silva

Received: 9 June 2009 / Accepted: 27 August 2010 / Published online: 16 September 2010

Abstract Stone masonry is one of the oldest building techniques used worldwide and it is known to exhibit poor behaviour under seismic excitations. In this context, this work aims at assessing the in-plane behaviour of an existing double-leaf stone masonry pier by experimental testing. Additionally, a detailed 3D finite element numerical analysis based on micro-modelling of the original pier is presented (fully describing the geometry and division of each individual elements, namely infill, blocks and joints) aiming at simulating the experimental test results. This numerical strategy can be seen as an alternative way of analysing this type of constructions, particularly useful for laboratory studies, and suitable for the calibration of simplified numerical models. As part of a wider research activity, this work is further complemented with the presentation of an effective retrofit/strengthening technique (reinforced connected plaster) to achieve a significant improvement of its in-plane cyclic response which is experimentally verified in the results presented herein.

Keywords Stone masonry · In-plane behaviour · Experimental test · Numerical modelling · Strengthening

1 Introduction

Post-earthquake surveys have often confirmed that traditional stone masonry buildings behave poorly under seismic motions, as observed recently in L'Aquila 2009 earthquake. A number of reasons can be pointed out to explain such an unsatisfactory seismic performance, namely the poor mechanical characteristics of mortar commonly used in these walls, the low shear

A. A. Costa (✉) · A. Arêde · J. Guedes · B. Silva
Department of Civil Engineering, Faculty of Engineering, University of Porto, Rua Dr. Roberto Frias, s/n, 4200-465 Porto, Portugal
e-mail: aacosta@fe.up.pt

A. Costa
Department of Civil Engineering, University of Aveiro, Campus Universitário de Santiago, 3810–193 Aveiro, Portugal

Fig. 1 Earthquake induced damages in Azores: **a** total collapse; **b** partial out-of-plane collapse; **c** in-plane damage

strength at the mortar-stone interface and the weak infill material properties. All these issues contribute for a non-monolithic behaviour of traditional stone masonry elements that can easily disaggregate when subjected to intense ground motions with some important vertical component. Besides, the partial or total collapse of these buildings is linked to in-plane and out-of-plane failure mechanisms that depend on the building characteristics (e.g., material properties, building configurations, connections between elements, inertial masses) and on surrounding elements (e.g., aggregate buildings, weak soils, etc.). Examples of different types of failure were observed during the 9 July 1998 Azores earthquake, where several masonry constructions behaved very badly leading to a significant number of total or partial collapses (Fig. 1). As a matter of fact, 2,100 buildings were destroyed and 2,900 severely damaged, from a total amount of 8,720 constructions (INE 2002; Neves et al. 2008).

Earthquakes generated in the Azores archipelago are mainly shallow crustal and characterized by moderate to high magnitude (Mw $\approx$ 6.0) with large peak ground accelerations. This particular earthquake included two features that were responsible for the amplification of its effects: the small distance to the fault (less than 10 km) and the significant peak ground acceleration ($PGA = 0.40$ g) with an important vertical component (0.33 g) (Oliveira and Malheiro 1999). In fact, this vertical component was correlated with the horizontal one due to the small distance to the fault, thus leading to quasi-simultaneous actions responsible for inducing strong damage on masonry constructions due to the uplift action that greatly reduces the shear capacity of masonry elements. In addition, the frequency content of this shallow crustal earthquake included important components matching the natural frequency range commonly found in this type of traditional masonry buildings, thus inducing severe excitation on such constructions.

The great heterogeneity of traditional Azorian masonry constructions, particularly those found in rural areas that constitute pieces of heritage to be preserved, makes them rather difficult to be reproduced in laboratory. Moreover, there is a clear lack of knowledge concerning material properties of such masonry elements as they exist in original in-situ conditions, for which experimental field tests are needed such as those reported in references (Costa 2002; Arêde et al. 2008). Complementarily, the opportunity of taking a masonry wallette from an existing traditional construction of the Faial Island, Azores, was found relevant for extracting useful information concerning physical and material properties of that masonry type concerning the in-plane response. Although (unfortunately) only one specimen was possible to be extracted and tested in laboratory conditions, still this research activity is thought to have provided good contributions for a good understanding of this material type

It is clear however, that, in general terms rather than the specific case of Azorian constructions, the study of the mechanical behaviour of traditional stone masonry elements is a key issue to understand their performance under future earthquake actions and to develop correct

and effective strengthening/retrofitting techniques. In this context, the present work can be seen as a further contribution to previous works carried out by the authors in the same area (Costa 2002; Costa and Arêde 2006), following the seismic event of 1998 on Azores islands.

This work can be regarded as featuring a comprehensive approach to assess the in-plane behaviour of stone masonry walls and to evaluate the effectiveness of a retrofitting strategy, while highlighting the applicability of numerical strategies to simulate experimental data. In this domain, different methodologies can be used for the numerical modelling of masonry structures, depending on the masonry typology and the study purposes.

Indeed, several different approaches and models were developed based on the finite element method (e.g. Page 1978; Lourenço 1996; Gambarotta and Lagomarsino 1997; Milani et al. 2006), the discrete element method (e.g. Cundall 1988; Lemos 2007) or macro-elements (e.g. Gambarotta and Lagomarsino 1996; Magenes and Della Fontana 1998). The best method for each study is the one that provides accurate and reliable information, by reproducing approximately the desired results, and that can be also adopted in other similar type studies.

In recent years, there has been an increasing interest on masonry characterization and retrofitting, particularly on stone masonry (e.g. Penazzi et al. 2001; Valluzzi et al. 2001; Magenes et al. 2009), due to its relatively poor behaviour under earthquake actions and to the fact that it is extensively used in seismic prone areas. The need to retrofit and strengthen this type of buildings is related to human loss reduction and to the architectural heritage preservation. Within this scope, a few works were recently done regarding traditional unreinforced masonry (URM) buildings (e.g. Sorrentino et al. 2008) and also focusing on the evaluation of retrofit and strengthening techniques resorting to composite materials (e.g. Juhásová et al. 2007; Corradi et al. 2008).

In this framework, the present research work aims also at discussing and assessing a strengthening technique that can be used on traditional stone URM buildings without significant costs to owners while keeping high benefit/cost ratios.

2 Experimental testing

2.1 Test specimen

As mentioned before, the seismic assessment evaluation of typical poor-type stone masonry of Azorian constructions was complemented by performing experimental laboratory tests on a real existing masonry pier recovered from a two storey house located at the Pedro Miguel parish, Horta council, Faial Island, hit by the 1998 Azores earthquake. This pier was located at the ground floor between two main doors of a house façade, as shown in Fig. 2.

This specimen is part of a traditional double-leaf stone masonry wall common to most of the old constructions in the Archipelago, mainly built of basalt blocks, cohesionless infill material (small stones, soil type material, etc.) and with an extremely poor bond between materials. It essentially consists of dry joints between basalt blocks and very weak joints between blocks and infill, as illustrated in the picture of the wall cross-section included in Fig. 2c.

Concerning foundations, it is worth mentioning that these constructions usually do not include any special element, being simply settled on the soil with some layered bottom blocks almost right below the ground level. This is a common situation because these buildings are usually low rise, so depending from the soil, they do not need very deep and large foundations.

Fig. 2 Original location of the wall: **a** general view; **b** pier location; **c** wall cross-section

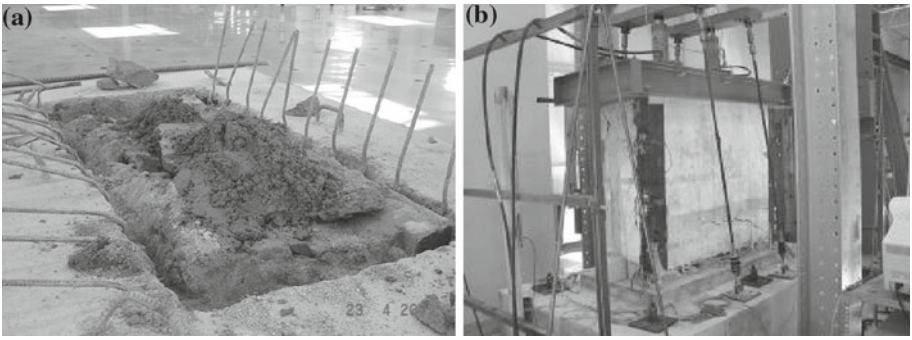

Fig. 3 Masonry pier preparation: **a** foundation; **b** installed specimen

2.2 Specimen preparation and test setup

Several steps were required in order to test the pier, starting with the cutting to extract it from the original house and the appropriate packing in a steel "boxed frame" for transportation to the Laboratory for Earthquake and Structural Engineering (LESE) at FEUP, Porto. After careful unpacking the pier was inserted in a pre-prepared basement aiming at reproducing adequately the in-situ foundation. This basement consisted on a concrete footing with a slot partially filled with a soft layer made of sand and stones as shown in Fig. 3a where the wall was settled; this leads to limited restrain capacity, especially concerning uplifting and shear at the base level, as required to appropriately account for the lack of adequate foundations of these buildings. All these operations were carried out with special care to avoid any damage on the specimen. A stiff mixed steel/concrete cap was then placed/casted at the top of the wall in order to distribute efficiently the vertical and horizontal loads to be applied during the test, as illustrated in Fig. 3b.

The tested pier was 1.475 m long in the outer face (1.36 m in the inner face), 0.70 m thick and 1.20 m high, leading to an approximate volume of 1.19 m^3.

In this work, the main concern focused on the in plane response of this type of walls as a complement to in situ tests previously made by the authors in similar walls of single storey houses. For these constructions, neither the roof/ceiling structures (made of wood improperly attached to walls) nor the masonry lintels above openings (doors or windows) are stiff enough to prevent top rotations of the wall. Based on this reasoning, a simple cantilever test setup was adopted to characterize the lateral in plane wall response fixed at the base and displacement/rotation free at the top (Costa 2007).

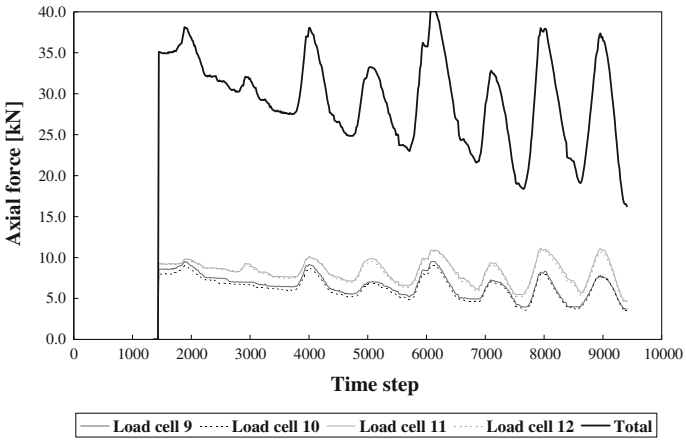

Fig. 4 Axial force during the experimental test

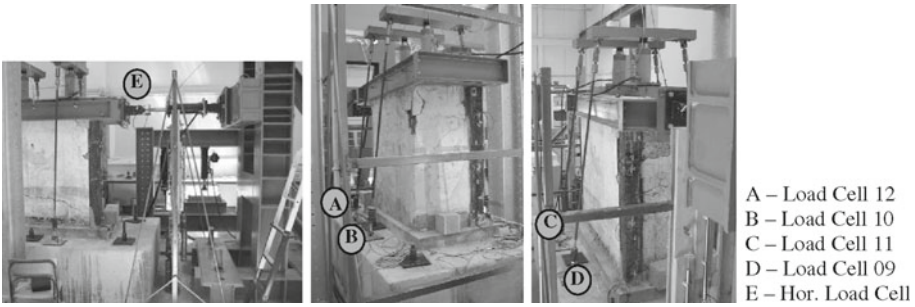

Fig. 5 Test setup and load application

In order to apply the vertical load, two hydraulic jacks were installed on the top, reacting against two steel beams connected to the wall foundation through hinged steel rods (Figs. 3b and 5), where load cells were installed to measure the imposed force. The applied vertical force (35 kN) was chosen so as to reproduce a realistic vertical load; according to the distribution of loads, such force accounted for the self-weight of the upper part of the wall and of the top timber roof.

However these hydraulic jacks were not force-controlled and, consequently, a significant variation of vertical compression was observed during the experimental test, as depicted in the time history of vertical load included in Fig. 4. This non-negligible load variation was due to absence of oil volume correction inside the hydraulic jacks to compensate for the cyclic uplifting and the progressive vertical deformation of the specimen. The peaks in the plots of Fig. 4 refer to the pier uplift, whereas the clear global decreasing trend is due to the average compressive deformation for which no correction was provided on the total axial force. For completeness, Fig. 4 includes records of each of the four load cells that are summed up to provide the total vertical force, corrected for the small angle of the steel rods where load cells where mounted on.

The horizontal load was applied by means of a displacement-controlled actuator connected to the top cap as shown in Fig. 5, introducing constant shear force along the wall length and height and linear variable bending moment in height down to the foundation.

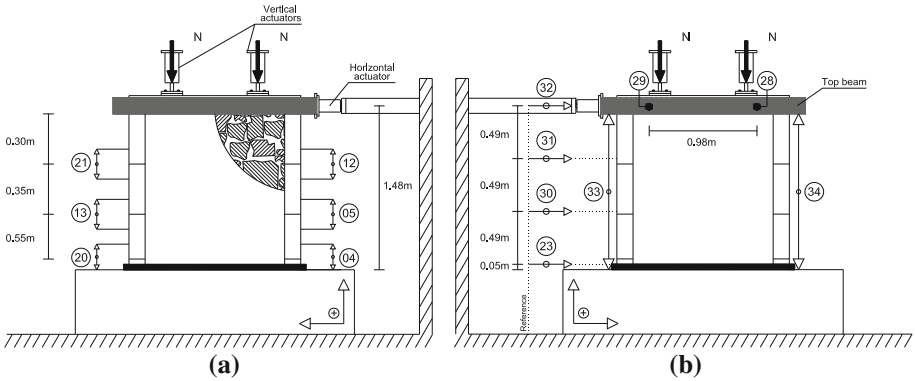

Fig. 6 LVDT's positioning: **a** front view (*outer face*); **b** back view (*inner face*)

Several displacement transducers were placed as illustrated in Fig. 6 for adequately monitoring the wall response by recording all possible movements. Horizontal LVDTs (Linear Variable Displacement Transformers) were placed at several in-height levels in order to obtain the deflected pier profile; global vertical deflections were also measured and complemented with more localized measures of joint opening-closing between blocks; out-of-plane movements were monitored with two LVDTs. Unfortunately, displacement measuring along the two diagonals was not possible due to instrumentation problems.

3 Test results

The experimental test was performed at constant velocity by imposing displacement controlled cyclic loads on the specimen, typically corresponding to three cycles for each desired target displacement. However, since the velocity initially introduced in the control program was considerably low, an extremely extended test time would be required and, therefore, it was decided to perform just one cycle per target displacement, thus reducing the test time to reasonable values. It is worth mentioning that this experiment has been one of the first cyclic tests carried out at LESE; the control and actuation system was not yet functioning in the desired conditions and some unexpected issues have occurred, such as non-symmetric displacement histories as shown below.

In order to allow for subsequent retrofitting of the wall and further testing, partial and severe collapse of the specimen was avoided by stopping the test when the maximum strength decreased by 15%, rather than 20% as commonly adopted in similar studies.

As a general remark, it should be referred that the tests presented were performed under quasi-static conditions in order to gather experimental results concerning material behaviour for this type of wall. However, it is recognized that it might not be the most adequate option to reproduce the dynamic loading response since damping effects can be modified under high frequency vibration, particularly the vertical one, among some other issues (e.g. loading rate) addressed in some other works (Paulson and Abrams 1990; Abrams 1996).

3.1 Global behaviour

The global behaviour observed in the specimen was essentially controlled by shear, as evidenced in Fig. 7b by diagonal and horizontal cracks along the bed joints. The crack pattern

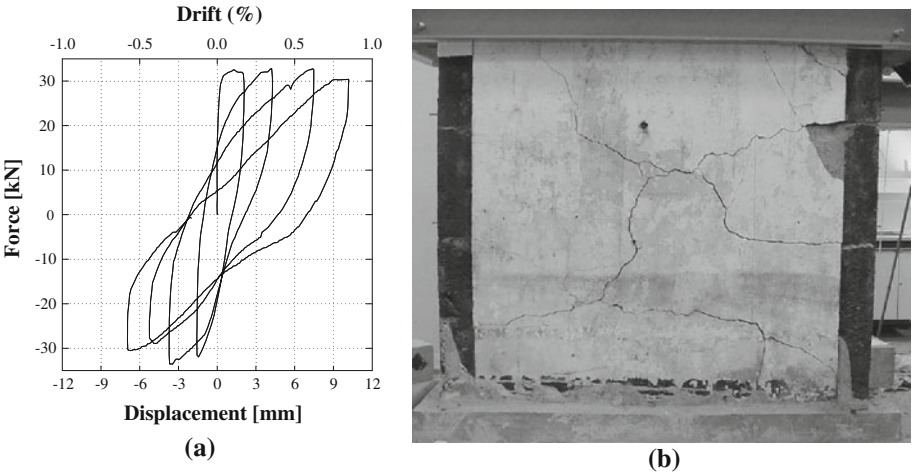

Fig. 7 Results obtained: **a** force vs. displacement curve; **b** cracking pattern

was governed by the stone block arrangement (presented clearly in Fig. 10a) since the cracks propagated around the basalt blocks due to poor connection between them and the infill material. It should be referred that the mortar cover was duly bonded to the wall and neither spalling, nor separation of wall leaves were observed.

This behaviour is consistent with the top force-displacement curve shown in Fig. 7a and the discontinuity surfaces with poor shear strength observed along the wall height. Besides the shear type behaviour of the tested specimen, (Fig. 7a) also evidences a significant amount of energy dissipation between each displacement level and non-negligible displacement ductility. However, the residual displacements on each cycle were considerably high, due to the behaviour mode (shear) and to the incapacity to recover displacements of this type of element.

The initial stiffness in the first branch progressively decreases due to the destruction of connections at the joints, for increasing displacement reversals. It is worth referring that if more cycles were performed per displacement level, a more severe damage would have been expected since significant strength decrease was observed for the same displacement level. In particular, from the 4 to the 6 mm loading cycle a local strength drop of about 20% occurred at 4 mm that was recovered at the cycle end, i.e. for 6 mm displacement. However, the last loading cycle shows that a non-recoverable strength loss occurred, since the curve seems incapable of reaching the strength capacity of the previous cycle.

The maximum strength achieved was 33.5 kN for a drift level of 0.1%, while the approximate limit of the elastic regime was found for about a 0.03% drift.

Despite the important influence of the axial load level on shear strength of masonry panels, it is possible to estimate the shear strength for similar wall elements. Therefore, by considering the full section contribution to shear distortion in agreement with the observed data in Fig. 7a (where the maximum strength is achieved for a very small displacement level) and consistent with a conservative approach, the maximum shear strength f'_v can be computed using Eq. (1). Adopting $A_s = 5/6A$, where A_s is the effective shear area, and $V_{\max} = 33.5\,\text{kN}$,

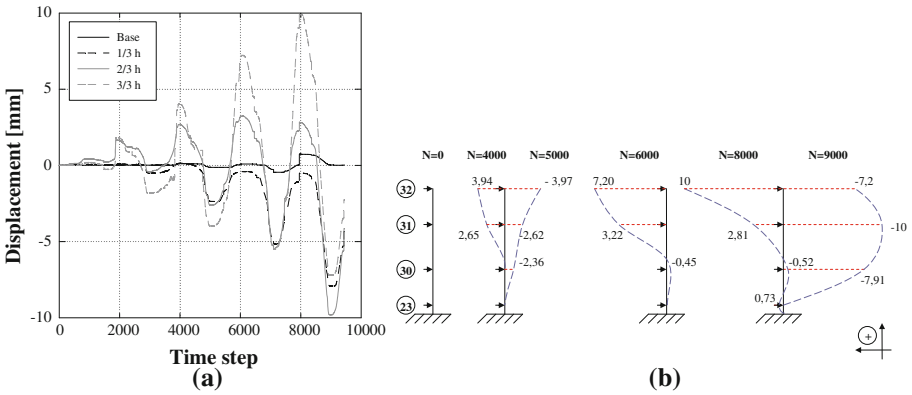

Fig. 8 Lateral displacements: **a** over time; **b** vertical profile

$$f_v' = \frac{V_{\max}}{A_s} \tag{1}$$

$$f_v' = 41 \text{ KPa}$$

It is worth mentioning that this value is in good agreement with the recommended values presented in relevant code standards, namely the Italian Seismic Code (OPCM no. 3274 2005) which, for a natural stone wall with external leaves and internal mixed filling, recommends values between 35 kPa $\leq f_v' \leq$ 51 kPa; this fact helps on highlighting the consistency of the obtained results.

3.2 Local behaviour

Despite the large amount of available test data, the information presented below refers to the opening/closure of joints and to lateral displacements along the wall height that are compared to the numerical results in Sect. 4. Resorting to the data recorded from readings of LVDTs n. 30, 31 and 32 presented in Fig. 6, the time histories of horizontal displacements at one third, two thirds and total wall height were plotted and included in Fig. 8a. In addition, (Fig. 8b) includes elevation displacement profiles for five time steps (4,000, 5,000, 6,000, 8,000 and 9,000).

From Fig. 8, it is possible to conclude that, despite some initial cohesive features, the wall has lost the bed joint cohesion, leading to a shear response characterized by sliding of the upper part of the wall over the middle part, as evidenced in Fig. 8b for time steps $N = 8{,}000$ and $N = 9{,}000$.

This behaviour is further highlighted in Fig. 9, where joint movements are plotted against the top displacement; these results show the response of LVDTs 13 and 5 as the most representative of shear/sliding behaviour with uplifting effect since the opening of joints has occurred for all peak displacements regardless of their sense. At the base level, there was no joint opening which means that no flexure/rocking response occurred; instead, the base joints (LVDTs 4 and 20) essentially moved towards closure due to the destruction of cohesion and to the smoothening of irregularities at this level. It should be also referred that results related to LVDT 12 are not presented due to the damage occurred at the top right corner of the wall that is possible to observe in Fig. 7b.

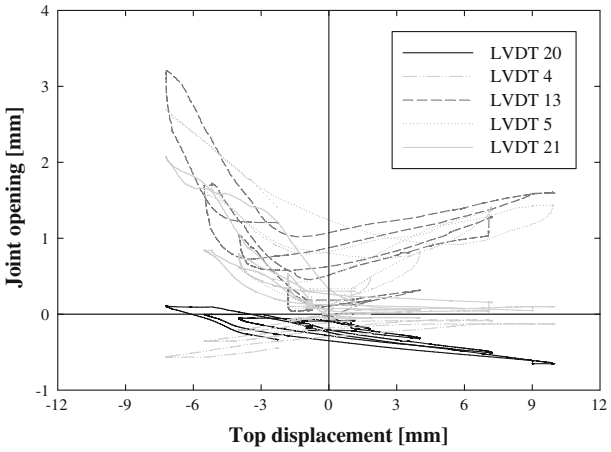

Fig. 9 Top displacement vs. joint opening

4 Numerical simulation

Numerical simulation of the experimental test was done aiming at applying and calibrating a modelling strategy to be used in other studies involving cyclic response of traditional masonry. In particular, the main objective of this numerical modelling strategy was to adopt a complex geometry but with simple behaviour models, thus requiring few mechanical parameters to be defined, in order to calibrate this type of simple model for use in future works.

In this context, instead of adopting a simplified geometric model with complex behaviour laws or homogenized models (such as the one proposed by Gambarotta and Lagomarsino 1997), or even rigid element models (e.g. Casolo and Peña 2007), a complex 3D and fully discretized finite element model was constructed to support simple material behaviour models.

The numerical modelling and computations were performed resorting to the general purpose finite element based computer code CAST3 M (CEA 2003) formerly known as CASTEM 2000.

4.1 Development and calibration

In order to obtain the best possible representation of the wall geometry, the plaster cover was completely removed after the test and the complete geometry was reproduced in a CAD program. Subsequently, the geometry was converted into a finite element mesh, where three different types of elements were generated, namely: 3D solid elements to represent both the basalt stone blocks and the infill zones and zero thickness joint elements to simulate block-to-block and block-to-infill interfaces. This allowed all materials and connections (represented in Fig. 10) to be adequately reproduced and modelled.

After completion of the numerical model geometry, a calibration process of the mechanical parameters was followed making use of both previous experimental tests (Costa 2002) and modal analyses results obtained from in-lab free vibration measurements of the wall without top beam, as illustrated in Fig. 11a. Results expressed in terms of FFT of acceleration signals in the transversal and longitudinal directions are included in Fig. 11b and c, showing the first two natural frequencies of the wall as 19.5 and 27.3 Hz, respectively for the transversal and longitudinal directions.

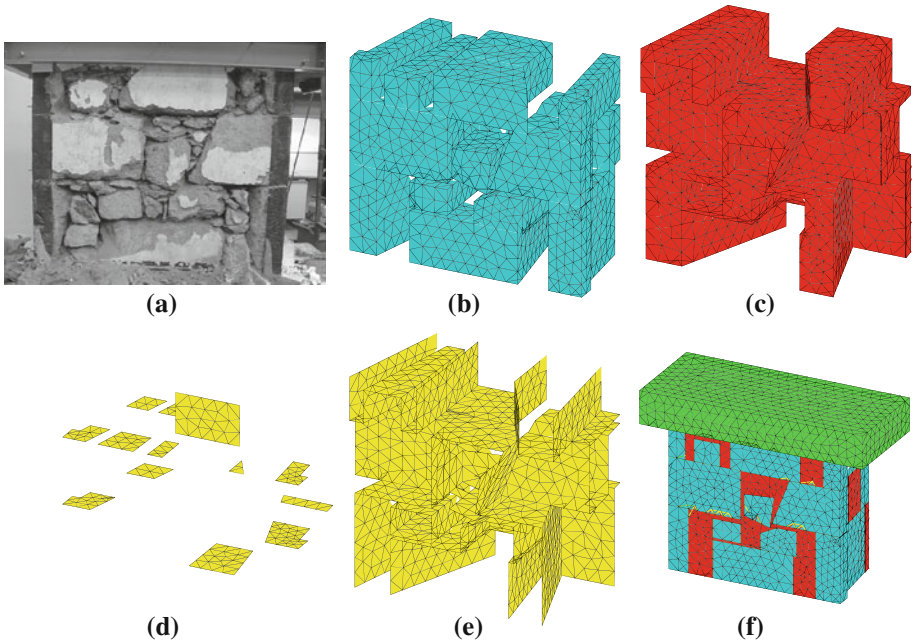

Fig. 10 Geometry of the wall: **a** real geometry; **b** stone blocks (FEM); **c** infill (FEM); **d** joints block-to-block (FEM); **e** joints block-to-infill; **f** complete FEM mesh

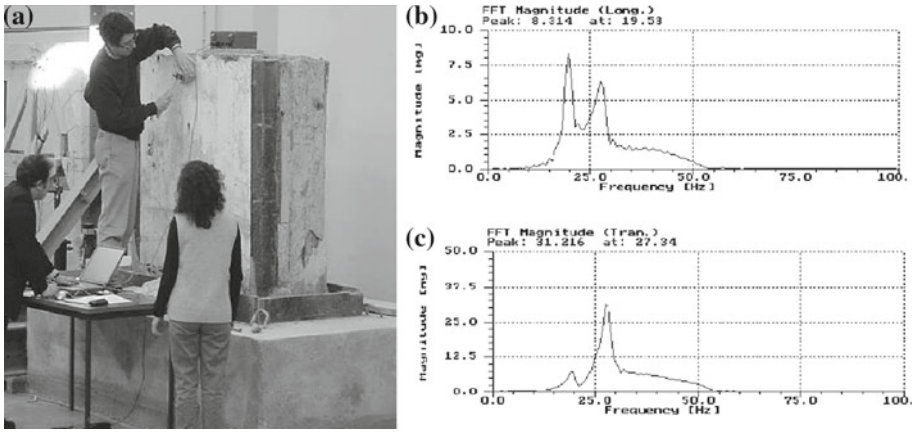

Fig. 11 Modal analysis: **a** free vibration test; FFT of acceleration record in **b** transversal and **c** longitudinal directions

Based on these results, the numerical model was calibrated in the linear elastic range of material behaviour in order to match the obtained first two modes of vibration presented in Table 1. This was done by taking values obtained by Costa (2002) for the blocks and infill; concerning the parameters for joints, the initial trial values were based on results of a previous work, where experimental shear tests on dry joints were carried out (Almeida 2000). Successive corrections led to the final joint parameter values used in the calibrated numerical model, listed in Table 2 together with the initial values.

Table 1 Modal frequencies comparison: experimental vs. numerical

	Experimental (Hz)	Numerical (Hz)
1stmode	19.5	19.7
2nd mode	27.3	27.3

Table 2 Mechanical parameters used in the numerical model and by Almeida 2000 (in brackets)

	Young modulus E (GPa)	Unit weight γ $\left(\mathrm{kN/m^3}\right)$
Blocks	28.7	26.0
Infill	0.25	18.0
Joints	Normal stiffness k_n (MPa/mm)	Shear stiffness k_s (MPa/mm)
Block/block	4.74 (6.24)	0.68 (0.68)
Block/infill	0.062 (0.032)	0.007 (0.038)

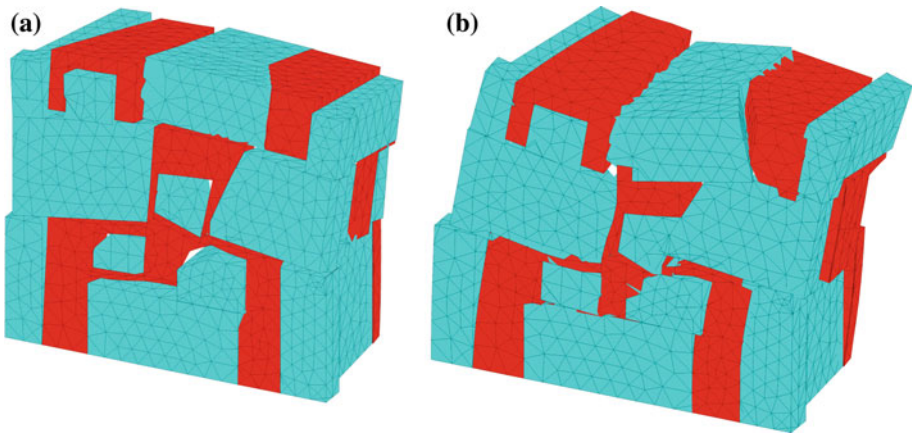

Fig. 12 Modes of vibration shapes: **a** 1st mode (*transversal*); **b** 2nd mode (*longitudinal*)

The first two vibration mode shapes obtained with the numerical model are illustrated in Fig. 12, where blue elements refer to basalt blocks and the red ones represent the infill; joint elements are not visible because they have zero thickness.

4.2 Non linear model characteristics

After the initial calibration of the material parameters, a non linear model was defined aiming at reproducing the experimental results by considering a non-linear behaviour of infill and joints. Actually, the blocks were considered to remain in the elastic regime, whereas the infill and joints were assumed to behave non-linearly because they are usually the weakest elements. This was confirmed during the test since no visible damage was found in the stone blocks.

For this purpose, the Drucker–Prager model implemented in CAST3 M (Drucker and Prager 1952; Duchesne and Raepsaet 1997), featuring an elastic-perfectly plastic (no hard-

Table 3 Nonlinear parameter values used for infill—Drucker–Prager model

f_t (kPa)	f_c (kPa)
10	32

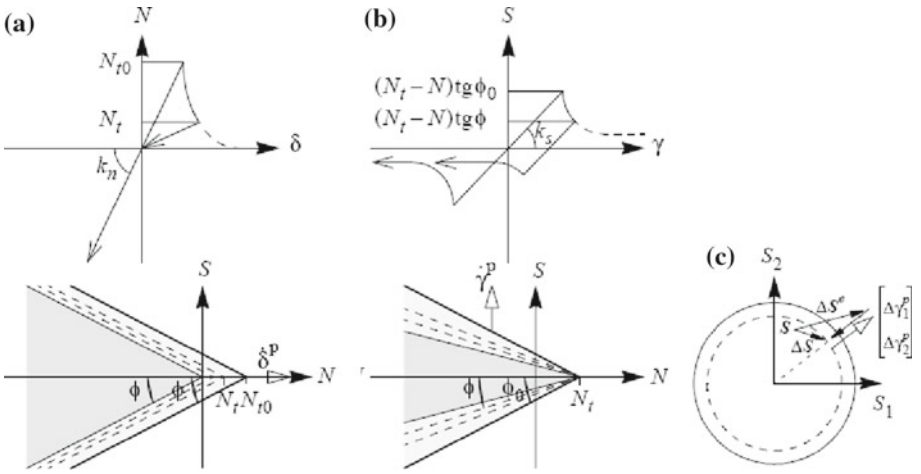

Fig. 13 Joint model (Pegon and Pinto 1996): **a** tension behaviour ($S = 0$); **b** shear behaviour ($N < N_t$); **c** radial return

ening) with associated plasticity model, was selected to simulate the infill behaviour due to its properties similar to a soil type material. In addition, two other reasons have justified this model selection: on the one hand, only two input parameters are required to define the yield surface (f_t and f_c—respectively, the uniaxial tensile and compressive strength), allowing for a faster calibration process compared to other more complex models; on the other hand, it avoids the need for hardening rule definition (difficult to give a correct characterization) thus reducing the number of parameters required to represent the nonlinear behaviour. Therefore, the nonlinear parameter values used in the numerical simulation of the infill are listed in Table 3.

It should be referred that the values presented in Table 3 may be presented in other terms, more precisely the cohesion and friction angle values, respectively, 7.7 kPa and 38°, similar to values found in literature (e.g. Cavicchi and Gambarotta 2005; Betti and Vignoli 2008).

Regarding the joint elements, the joint softening model as implemented in CAST3M (Pegon and Pinto 1996) was used. The model was adopted after the nonlinear calibration performed by Almeida (2000) and it was adjusted to better simulate the experimental results.

This model features a purely dilatant plastic flow rule with kinematic softening for tension failure, as schematically described in Fig. 13a, while for pure shear failure a dilatancy-free plastic flow rule with softening is adopted (Fig. 13b). Tension and shear behaviour coupling is only activated through the cohesion that affects both the shear and tension responses. A radial return algorithm expresses the reduction of elastic stress overshoot and the plastic flow, following the direction orthogonal to the Coulomb cone axis, as exemplified in Fig. 13c.

Hence, two different behaviour rules are required for the model, namely for normal (tensile) and shear stresses acting in the joint. However, for the case under analysis, no tensile strength was considered in the joints, a typical assumption for poor/dry joints as the case of this masonry wall. Concerning shear behaviour, a multi-linear rule could have been defined

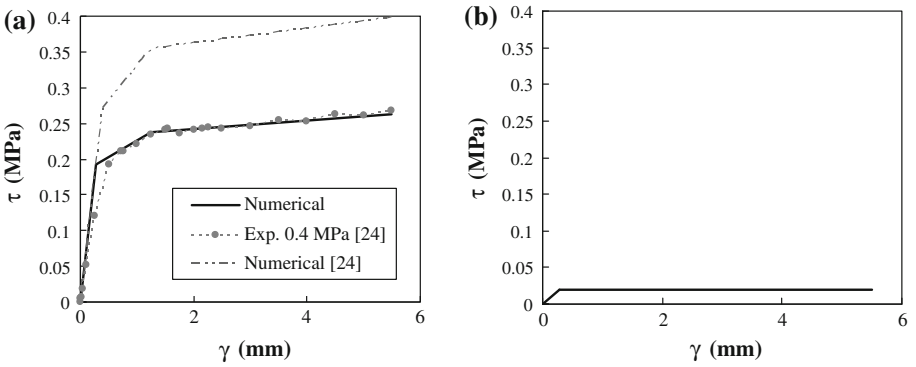

Fig. 14 Nonlinear shear behaviour of joints: **a** block-to-block; **b** block-to-infill

in order to characterize properly the initial stiffness, the peak strength and the post peak behaviour, as schematically depicted in Fig. 13b. However, it was found more realistic to assume that the peak strength had been already achieved during the earthquake and/or the management and transportation of the wall, since it is quite logical to accept that such facts were sufficient to destroy the initial friction between elements. This reasoning supports the assumption of elasto-plastic shear behaviour for block-to-infill joints and trilinear response curve with hardening for block-to-block (Pegon and Pinto 1996).

In order to calibrate the nonlinear parameters for block-to-block joints, the normal stress distribution at the joints due to self weight was analysed through a simple linear static analysis with the material parameter values presented in Sect. 4.1, thus leading to normal stress values between 0.25 and 0.5 MPa. Therefore, the nonlinear range of the trilinear rule was adjusted on the basis of experimental tests reported (Almeida 2000) for a normal stress level of 0.4 MPa as shown in Fig. 14a which includes both the numerical curve used in the presented work and also the trilinear rule used by Almeida (2000) for normal stress of 0.6 MPa. Regarding the nonlinear shear behaviour of the block-to-infill joints, the initial stiffness was defined by modal calibration (as described in Sect. 4.1), while the plastic plateau was selected to match the experimental results of the masonry wall, leading to the final curve depicted in Fig. 14b.

Finally, it is worth mentioning that the top stiff concrete cap was also included in the numerical model, though considering it behaving linearly with an elastic modulus $E = 100$ GPa and an unit weight $\rho = 29.7\,\text{kN/m}^3$. These values were deliberately taken large in order to simulate a very stiff element to ensure uniform load distribution in the wall.

4.3 Numerical results

The imposed vertical loads were obtained from the experimental test, meaning that the axial force variation was also taken into account in the numerical analysis in order to simulate accurately the experimental test. Similarly, the imposed displacements in the simulation are exactly the experimental ones by adopting the same displacement increments levels as in the test.

The numerical simulation was carried out on the calibrated model as described in Sec. 4.1 and the infill nonlinear parameters were adjusted to better match the experimental results resorting to a trial and error process (with the final values listed in Table 3), which led to final numerical results very close to the real ones as shown in Fig. 15.

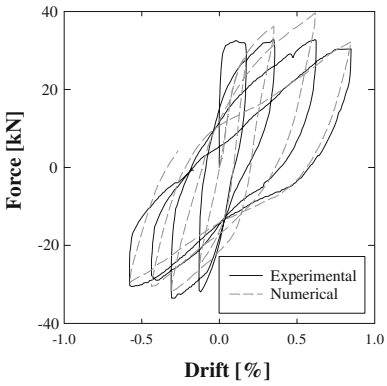

Fig. 15 Force drift diagrams: Experimental compared to numerical results

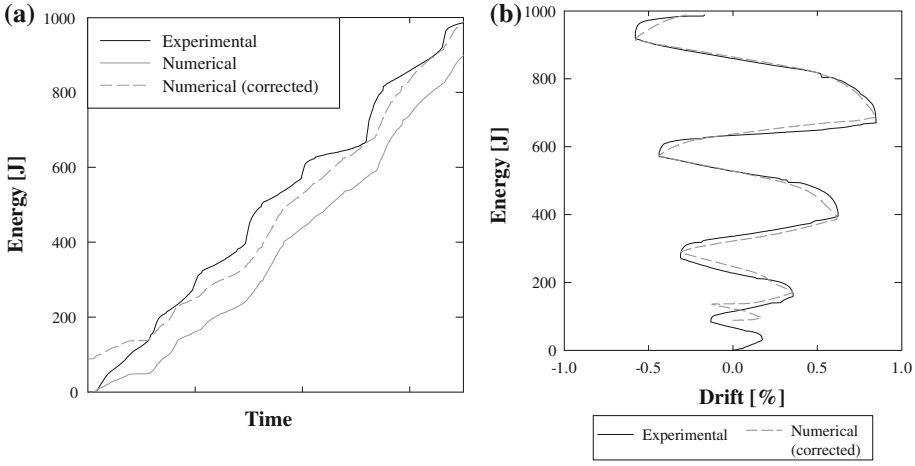

Fig. 16 Dissipated energy comparison: **a** dissipated energy vs. time; **b** dissipated energy vs. drift

The simulation output evidences that the hysteretic behaviour is globally well described by the model, since it is able to approximately reach the maximum strength (although slightly overestimated), also accounting for the observed stiffness/strength decrease and dissipated energy. Indeed, a comparison between energy dissipation capacity of the numerical and real model is presented in Fig. 16, confirming the accuracy of the numerical simulation.

Figure 16a shows the time history of dissipated energy, evidencing that in the initial part of the test the numerical model underestimates the dissipated energy. This is explained by the difficulty of the model to reproduce the initial stage of the test mainly influenced by the destruction of cohesion in bed joints. However, the model accurately reproduces the dissipated energy after this initial stage, as confirmed in Fig. 16b where a very good agreement is found between numerical and experimental results in terms of energy versus drift. In this Fig. 16b, the curve was shifted to match the final energy dissipation (also represented in Fig. 16a), highlighting the agreement between the numerical and experimental result.

Beyond this global comparison with the test results, the use of micro-modelling approach also allows comparing numerical and experimental findings concerning lateral displacements along the height (1/3 and 2/3 of total height), as well as out-of-plane displacements exhibited by the tested specimen (monitored by LVDTs 28 and 29 shown in Fig. 6); these further

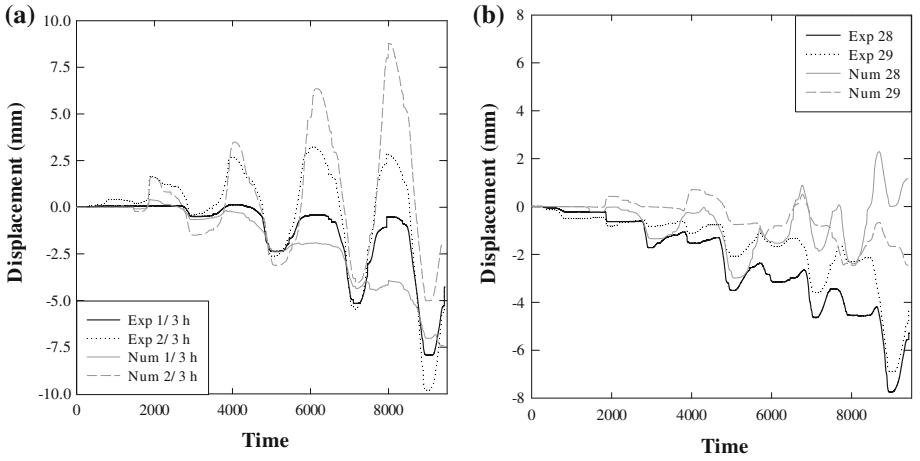

Fig. 17 Comparison of numerical with experimental displacement results: **a** lateral displacements; **b** out-of-plane displacements

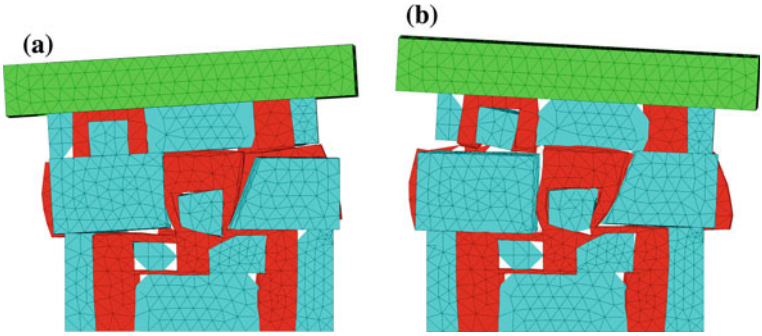

Fig. 18 Deformed shapes for maximum displacement: **a** positive (+10.0 mm); **b** negative (−7.5 mm)

comparisons are presented in Fig. 17. Results show that, at local level, the numerical model is less accurate and only partially reproduced the experimental results in terms of the wall displacements (up to the last third of the test).

Despite the differences found between the numerical model and the observed results, the general behaviour was correctly simulated and other interesting outputs were additionally put into evidence, such as the formation of preferential sliding surfaces shown in Fig. 18 and the dilatancy effects. Actually, Fig. 18 clearly exhibits a disconnection between the bottom layer of blocks and the middle-upper part of the wall, due to the existence of a quasi-continuous sliding surface. Moreover, it allows confirming that the wall behaviour is strongly influenced by the infill properties rather than the blocks, as evidenced by the separation between infill and blocks as well as the destruction of the connection between leafs (Fig. 18); this confirms the infill as the weakest element that essentially rules the wall response mechanism.

One of the main advantages of using micro-modelling of elements or structures is the possibility of deeply analyzing their behaviour resorting to different numerical results, such as the detailed deformed shapes like those presented above. Similarly, other interesting numerical findings were obtained with the principal stresses diagrams, where clear stress paths

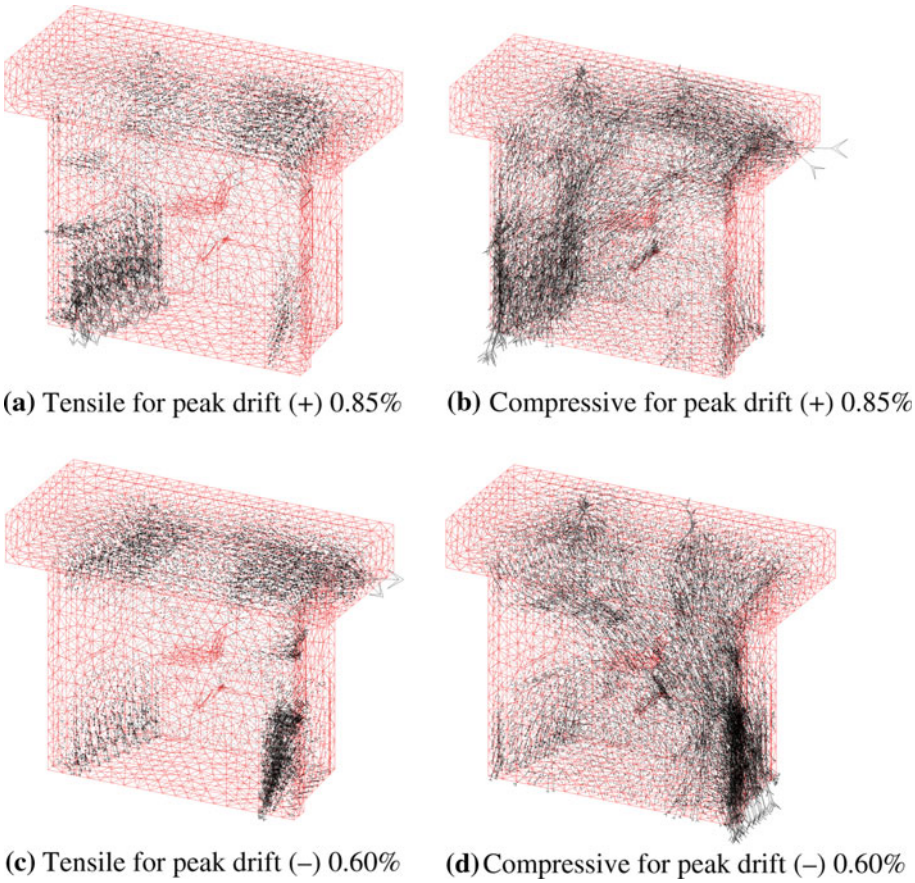

Fig. 19 Principal tensile and compressive stress distributions: **a** and **b** for peak positive displacement, **c** and **d** for peak negative displacement

can be observed throughout the wall as evidenced in Fig. 19 concerning the distribution of principal tensile and compressive stresses over the entire wall for the peak positive and negative displacements (0.85 and −0.6% drifts).

Actually, Fig. 19 puts into evidence the importance of a good infill material for this type of walls. It is clear that, despite the negligible contribution of the infill to tensile stresses (consistent with the very low tensile strength as adopted), the infill compressive strength is very important to allow the formation of a compressive strut through the wall core. This finding is quite clear in Fig. 19b and d, with the principal compressive stresses path mainly concentrated throughout the infill (further evidenced on Fig. 20, restricted to the infill zone mesh), while the stone blocks are particularly important for the connection to the foundation.

Finally, an additional numerical simulation of the experimental test under constant vertical load was also performed in order to study the influence of vertical load variation on the final results. The same calibrated model parameters were used as for the final results above described. Results for this simulation are shown in Fig. 21, in terms of global force-drift diagrams compared against the numerical output under the real vertical load (Fig. 21a) and the experimental response (Fig. 21b). These comparisons allow concluding that the vertical load

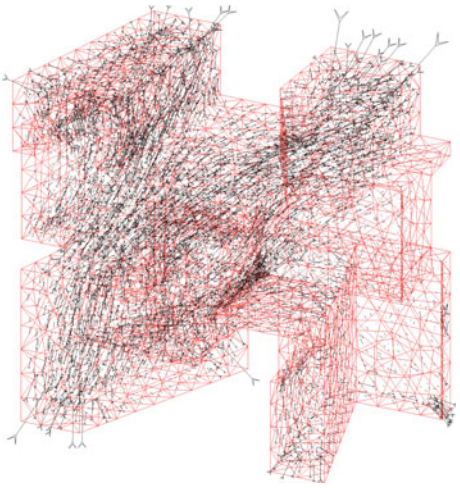

Fig. 20 Principal compressive stress path in the infill for peak positive displacement

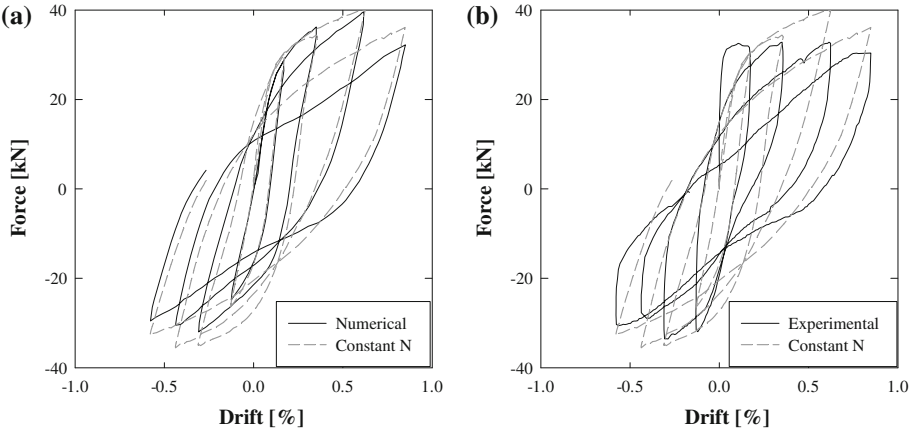

Fig. 21 Numerical results from constant vertical load simulation compared with: **a** numerical results from actual vertical load; **b** experimental results

variation did not influence significantly the final results because the variation amplitude was not large enough to modify the response mechanism (shear type) and the energy dissipation capacity. However, slightly larger maximum strength should be expected with lower strength decay after peak force.

5 Strengthening and subsequent testing of the specimen

Within the experimental activity herein reported, the masonry wall was afterwards retrofitted and strengthened following the same technique as used in Faial and Pico islands, Azores, after the 1998 earthquake, and tested again for assessing the efficiency of that technique during future seismic events. As explained by Costa and Arêde (2006), this retrofit/strengthening strategy essentially consists in a sort of reinforced cover jacketing (using mortar, surface mesh and connecting rods as explained below) that modifies a heterogeneous masonry wall

into a more homogeneous masonry block, likely to behave monolithically when subjected to horizontal excitations.

5.1 Retrofitting technique

The retrofitting technique used in the masonry wall is the same as used on several damaged structures in Azores after the 1998 earthquake. Although having been adopted for retrofitting after a seismic occurrence, clearly it can be also used as a strengthening method for existing buildings requiring improvement of seismic performance (Costa and Arêde 2006). In this context, the option by strengthening resorting to reinforced plaster becomes quite attractive for these traditional constructions, typically own by people with low economic resources, since it does not change significantly the original appearance and it presents itself as an economically viable and convenient solution rather than other strengthening/retrofitting techniques (e.g. grout injection). However, it should be also referred that the application of this technique should be complemented with other strengthening techniques in order to improve the global seismic behaviour, namely the connection between horizontal and vertical elements and between orthogonal walls both in corners and wall intersections. In such case, the response of the strengthened construction will be driven by a global behaviour due to a more homogeneous and well connected structure instead of being determined by local failure of single elements.

In what concerns historical constructions, the application of this technique should be avoided and resort should be made to other strengthening techniques liable to provide sufficient seismic resistance. Therefore, it is recognized that the intrusive nature of this technique makes it less interesting for historical constructions wherein its application should be considered as the last option for ensuring the required seismic resistance.

The *modus operandi* of this technique can be divided into ten different and simple steps, alphabetically labelled and presented in Fig. 22 as follows: (a) cover removal; (b) definition of the positions of transversal steel rods (red circles), with an approximate spacing of 50 cm although dependent also in the stone arrangement; (c) placing transversal rods to ensure connection between leafs; (d) filling joints with mortar; (e) installation of the steel mesh; (f) placing the steel plates and tightening of transversal rods to distribute their efficiency; (g) installation of a second layer of steel mesh above the plates; (h) cutting the excess of steel rods; (i) plastering with typical Azorian mortar cover; (j) mortar curing simulating Azores' humidity.

The application of this technique should be closely supervised since its efficiency is ensured by a proper application. This technique was applied in Italy and is recommended in the Italian Code but, as recognized by Penazzi et al. (2001), the detailing is very important to ensure the desired strength and ductility for seismic resistance. The main problems found in the cited work were as follows: lack of continuity between orthogonal walls and between floors and walls; deficient steel mesh overlapping; excessive spacing of transversal connectors; use of short connectors; insufficient mortar cover causing steel mesh corrosion; lack of uniform distribution of the repaired areas.

5.2 Experimental test

In order to assess the efficiency of the retrofit/strengthening technique, a subsequent experimental test was prepared based on the previous one (unreinforced specimen).

Fig. 22 Retrofitting technique used on the tested pier: from **a**–**j** as detailed in the text

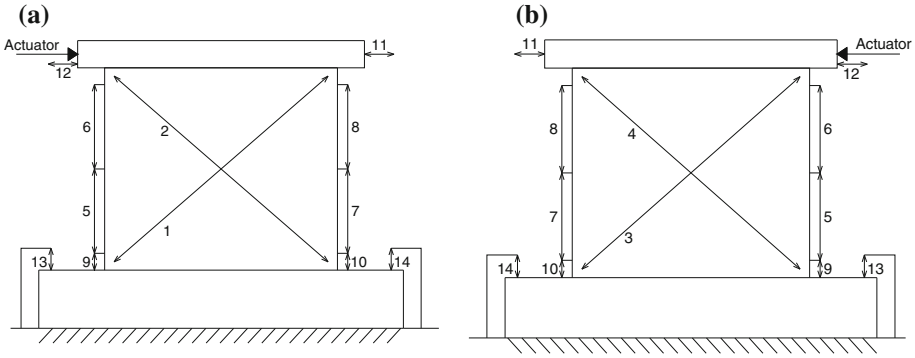

Fig. 23 Monitoring LVDTs on the retrofitted specimen: **a** front view; **b** back view

However, this second experimental activity can be considered as a set of three different experimental tests, corresponding to three different axial load levels that were successively applied to the same specimen in three distinct test stages. It should be referred also that, in opposite to the URM experiment, the axial load value was kept constant during each test stage. Thus, starting from 40 kN (approximately the original axial load), two other test stages were accomplished with 100 and 160 kN vertical force (respectively, 2.5 and 4 times the basic axial load). The objective of adopting these axial load levels was to assess the behaviour of the specimen subjected to different failure modes, expecting to change from flexural—rocking (observed at the lowest axial load level) to diagonal—shear cracking.

Hence this test started with the same target displacements as for the original test, but larger displacements were in fact imposed due to the actually observed behaviour and performance of the wall, as described in the next section.

Regarding the monitored points during the experimental test, a slight modification was made aiming at measuring possible shear distortion (LVDTs 1, 2, 3 and 4 in Fig. 23) and rocking motion of the foundation (with LVDTs 13 and 14).

5.3 Test results

Results obtained from the tests on the retrofitted masonry wall are depicted in Fig. 24 for the three different levels of the considered axial load (40, 100 and 160 kN). Additionally, bilinear idealizations of the response are also included in order to obtain displacement ductility capacity for each axial load level as also as to evaluate modifications on the equivalent stiffness.

Figure 24 allows concluding that the retrofitted specimen behaved monolithically exhibiting pure rocking with low energy dissipation. It should be mentioned, however, that the maximum imposed displacement for the axial load of 100 kN was lower than the other ones because the observed behaviour for this axial load level was similar to the previous test (N=40 kN), for which a rocking motion governed the response. Indeed, the axial load increase did not change the specimen behaviour and, therefore, the test was stopped before the target displacement and the vertical load was further increased aiming at obtaining a different behaviour mode (by diagonal cracking).

The general trend shows that the maximum displacement obtained for each axial load level did not have strength decrease or larger hysteresis, which is consistent with the material integrity of the wall.

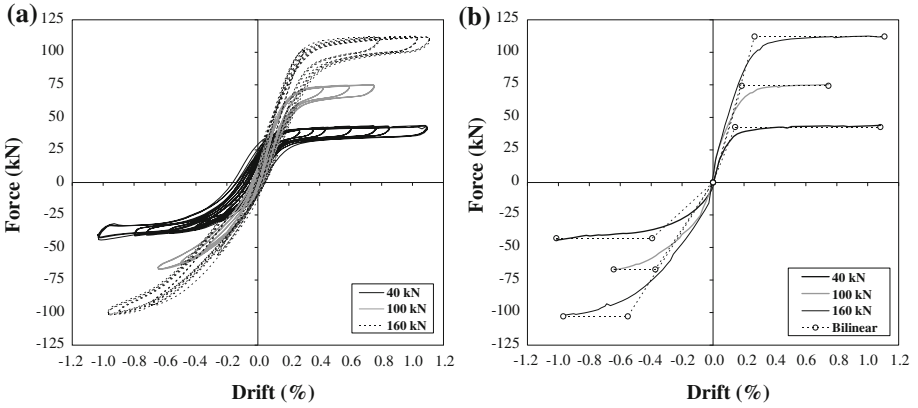

Fig. 24 Experimental test result—retrofitted specimen: **a** hysterisis loops; **b** envelopes with bilinear idealizations

For the first axial load level ($N = 40$ kN) the maximum strength reached 42 kN, i.e, 30% larger than the value of 32 kN obtained with the original specimen. The maximum drift reached 1.1%, but it was clear that larger displacements could have been imposed without any problem. Using a bilinear idealization of the response based on the Italian Code proposal (OPCM no. 3274 2005), more consistent than Eurocode 8 (CEN 2005) for masonry structures as reported (Costa 2007), an apparent displacement ductility capacity (μ_Δ) of 6.5 is found for this axial load level in the positive sense. It is worth noting that, for this rocking behaviour type, similar results should be obtained using the recent proposal by Costa (2007) and EC8 approach. In the negative sense, the maximum strength seemed to not be achieved, being the comparison of the displacement ductility not viable.

By increasing the axial load up to 100 kN, a maximum strength of 75 kN was achieved with the same rocking behaviour. However, due to the small amount of imposed displacement levels as explained previously, a comparison of the involved displacement ductility is not meaningful.

The larger level of axial load (160 kN) increased the maximum specimen strength up to 112 kN and imposed a displacement ductility of 4.1 in the positive sense (for the same maximum displacement level), lower than before due to the yielding point shifting. In the same line as in the 40 kN case, the maximum resistance was not achieved in the negative sense. However, it was clear that displacements could be easily increased because the specimen remained undamaged with displacement capacity significantly improved, which would lead to larger displacement ductility values. The energy dissipation capacity remained similar with this axial load level, mainly due to the rocking mechanism.

Another interesting result was obtained from the analysis of the diagonal and base joint displacement transducer readings plotted in Fig. 25 in terms of top drift vs. diagonal or base joint motion (opening or closing). These results are fully consistent with the observed monolithic behaviour of the wall, also inferred from the response diagrams included in Fig. 24 that are typical of a rigid block type.

Indeed, Fig. 25a shows the evolution of the diagonal displacements of the wall that is directly related to the shear influence on the global response; it is quite apparent that considerably low displacement values were found (maximum = 0.30 mm), allowing to conclude that shear behaviour did not influence the wall response. Similarly, Fig. 25b exhibits the joint

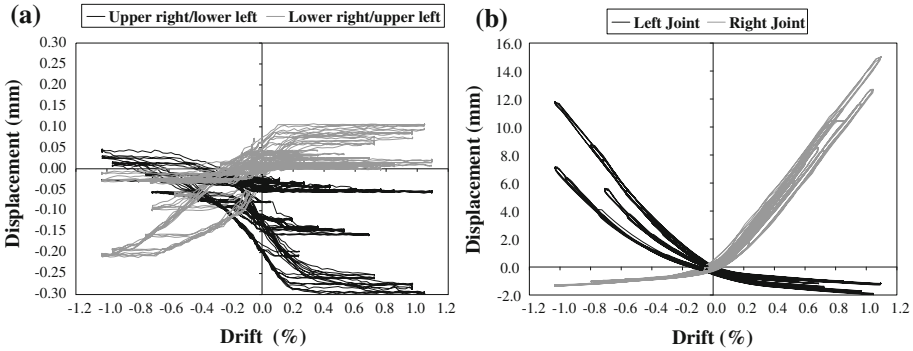

Fig. 25 Retrofitted pier behaviour: **a** diagonal displacement; **b** base joints opening

opening/closing during the experimental test, where the rocking behaviour is perfectly clear also in accordance with Fig. 24.

The largest displacement level achieved during the test yielded a maximum drift of 1.1%, but higher drift levels could be easily achieved due to the absence of damage in the wall for this displacement level (no toe crushing occurred). Actually, the test was stopped because no larger axial load could be applied due to limitations of the test setup (more precisely the top reaction steel elements), and the desired diagonal/shear cracking failure mode required higher levels of axial load to be activated.

As expected, the peak strength exhibited by the specimen increased significantly with the increase of axial load; the initial stiffness was also visibly changed.

The efficiency of this retrofitting technique was assessed because higher strength and displacement capacity were achieved, thus indicating that severe structural damages can be prevented. However, the energy dissipation capacity is clearly reduced when compared to a shear type failure due to the modification of behaviour mode into a rocking type mechanism. This means that improvements on this strategy can be of great added-value, for instance by introducing adequate connection to the foundation likely to reduce the rocking mode and to provide additional capacity of energy dissipation. This issue is being addressed by the authors resorting to in-situ tests of similar type masonry panels of existing structures, from which quite promising results have been already obtained (e.g. Arêde et al. 2008).

Finally, this technique avoids disaggregation of the masonry components or separation of the wall sleeves, inducing a more uniform in-plane behaviour. Furthermore, when applied to a complex structure, this technique should lead to a more efficient and predictable structural response with walls interacting as solid blocks.

6 Discussion

The work herein described has allowed assessing three different topics, namely: the in-plane behaviour of traditional stone constructions, particularly of Azores islands; cyclic response simulation using numerical modelling; the efficiency of a retrofit and strengthening technique used after the 1998 Azores earthquake.

The in-plane behaviour exhibited by the tested specimen was good concerning energy dissipation, but it was achieved through a non-ductile and not controlled behaviour mechanism essentially based on shear response. Although only one cycle per displacement level has

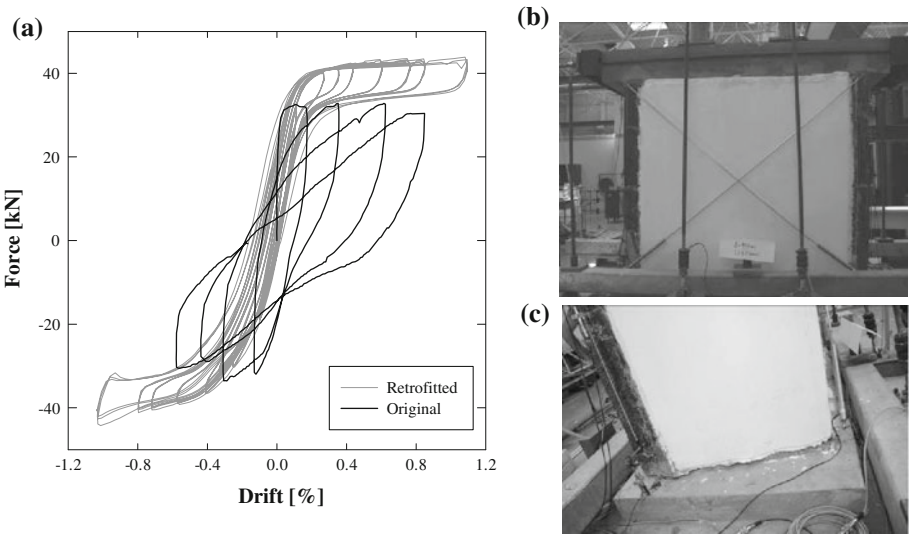

Fig. 26 Retrofit efficiency: **a** original vs. retrofitted results, **b** global and **c** local views of final stage of retrofit test

been actually performed, the post-peak strength decrease was significant (to about 80–85%) for maximum drift level of 0.85%. Moreover the wall did not keep its integrity during the in-plane loading, which was in fact one of the main problems related to the strength decrease (about 20%) for a constant displacement level. Therefore, it is possible to conclude that the wall did not behave satisfactory during the test.

Regarding the numerical modelling, it was possible to verify that, using a micro-modelling approach, the numerical analysis was able to simulate adequately the tested specimen response, as shown in Fig. 15. Despite the complexity of the geometric model, the complete discretization of the wall allowed assessing local displacements, amongst some other information not presented in this paper.

Finally, concerning the retrofit efficiency, a pertinent final comparison between the responses of the original wall vs. the retrofitted specimen is shown in Fig. 26, for the same axial load level.

It can be observed that the modification of the wall behaviour has changed completely the energy dissipation capacity, the maximum drift reached (retrofitted: 1.15% vs. original: 0.85%) and the wall integrity, bearing in mind that larger displacements could be easily achieved with the retrofitted specimen as explained before. Thus, it can be concluded that this retrofit/strengthening technique, used in Faial and Pico islands after the 1998 Azores earthquake, is adequate and effective to ensure the integrity of the wall as evidenced in Fig. 26b and c where no damage is found in the wall, except in the connection to the foundation. In addition, since this technique was adopted in-situ for all the elements in a given building, rather than just on piers or spandrels, a good behaviour of the complete structure may be expected with more energy dissipation.

7 Conclusions

A general overview including different topics was performed on this work, starting with the experimental in-plane behaviour characterization of a stone masonry wall, proceeding with

a complex numerical modelling of the tested specimen and, finally, assessing the efficiency of a retrofit/strengthening technique.

The experimental test allowed observing that the behaviour of traditional stone masonry walls is mainly controlled by shear due to poor joint shear strength and material heterogeneity. However, this behaviour may be substantially improved if an adequate strengthening technique is implemented to ensure a homogenous behaviour given by re-plastering of the wall with a mesh reinforced cover complemented with suitable connection between walls leafs. Although not addressed herein, the infill improvement with some sort of grouting is likely to add a significant positive contribution to the global behaviour of the wall.

Concerning numerical simulation, it can be concluded that the behaviour of a traditional stone masonry wall may be satisfactorily reproduced by micro-modelling of the complete geometry and making use of nonlinear models for the joints and infill. Although this was done for a tested specimen, thus with completely known response to a prescribed cyclic load, this achievement is considered important for future calibration of simpler models or even to model complete structures of similar type masonry.

Acknowledgments The authors would like to acknowledge some important persons that helped performing this work since the very first stage, namely Ms. Daniela Gloria and Mr. Valdemar Luis from the Laboratory for Earthquake and Structural Engineering (LESE) of the Faculty of Engineering of the University of Porto (FEUP), and Ms. Cristina Costa for great help concerning the numerical modelling. This work refers part of research made with financial contribution of the Portuguese Foundation for Science and Technology (FCT).

References

Abrams D (1996) Effects of scale and loading rate with tests of concrete and masonry structures. Earthq Spectr 12(1):13–28. http://dx.doi.org/10.1193/1.1585866

Almeida C (2000) Análise do Comportamento da Igreja do Mosteiro da Serra do pilar sob a Acção dos Sismos. MSc Dissertation. Faculdade de Engenharia da Universidade do Porto. Available via NCREP/FEUP. http://ncrep.fe.up.pt/

Arêde A (2008) In situ testing of the out-of-plane capacity of traditional stone masonry walls. International Seminar on Seismic Risk and Rehabilitation, Faial, Azores, Portugal

Arêde A, Costa A, Costa AA, Oliveira CS, Neves F (2008) Experimental in-situ testing of typical masonry constructions of Faial Island—Azores. In: 14th world conference on earthquake engineering. Beijing, China

Betti M, Vignoli A (2008) Modelling and analysis of a romanesque church under earthquake loading: assessment of seismic resistance. Eng Struct 30:352–367. http://dx.doi.org/10.1016/j.engstruct.2007.03.027

Casolo S, Peña F (2007) Rigid element model for in-plane dynamics of masonry walls considering hysteretic behaviour and damage. Earthq Eng Struct Dyn 36:1029–1048. http://dx.doi.org/10.1002/eqe.670

Cavicchi A, Gambarotta L (2005) Collapse analysis of masonry bridges taking into account arch-infill interaction. Eng Struct 27:605–615. http://dx.doi.org/10.1016/j.engstruct.2004.12.002

CEA (2003) Manuel dútilisation de Cast3 m, Saclay: Commissariat à l'Énergie Atomique. Available via CEA. www.cast3m.cea.fr

CEN (2005) Eurocode 8: design of structures for earthquake resistance, part 1: general rules, seismic actions and rules for buildings. Brussels, Belgium

Corradi M, Tedeschi C, Binda L, Borri A (2008) Experimental evaluation of shear and compression strength of masonry wall before and after reinforcement: deep repointing. Constr Bldg Mat 22:463–472. http://dx.doi.org/10.1016/j.conbuildmat.2006.11.021

Costa A (2002) Determination of mechanical properties of traditional masonry walls in dwellings of Faial Island. Azores Earthq Eng Struct Dyn 37:1361–1382. http://dx.doi.org/10.1002/eqe.167

Costa A, Arêde A (2006) Strengthening of structures damaged by the Azores earthquake of 1998. Constr Bldg Mat 20:252–268. http://dx.doi.org/10.1016/j.conbuildmat.2005.08.029

Costa AA (2007) Experimental testing of lateral capacity of masonry piers. An application to seismic assessment of AAC masonry buildings 2007. MSc Dissertation. European school for advanced studies in reduction of seismic risk (ROSE School)

Cundall PA (1988) Formulation of a three-dimensional distinct element model—part I: a scheme to detect and represent contacts in a system composed of many polyhedral blocks. Int J Rock Mech Min Sci 25:107–116. http://dx.doi.org/10.1016/0148-9062(88)92293-0

Drucker DC, Prager W (1952) Soil mechanics and plastic analysis or limit design. Quart Appl Math 10: 157–165

Duchesne A, Raepsaet X (1997) Un modèle Élasto-plastique de CASTEM 2000 utilisable pour la modélisation du comportement mécanique d'Un lit de particules. JRC, Ispra

Gambarotta L, Lagomarsino S (1996) On dynamic response of masonry panels. In: National conference "Masonry Mechanics Between Theory and Pratice". Messina, Italy

Gambarotta L, Lagomarsino S (1997) Damage models for the seismic response of brick masonry shear walls. Part II: the continuum model and its applications. Earthq Eng Struct Dyn 26:441–463. http://dx.doi.org/10.1002/(SICI)1096-9845(199704)26:4<441::AID-EQE651>3.0.CO;2-0

INE (2002) Censos 2001. Lisboa

Juhásová E, Sofronie R, Bairrão R (2007) Stone masonry in historical buildings—ways to increase their resistance and durability. Eng Struct 30:2194–2205. http://dx.doi.org/10.1016/j.engstruct.2007.07.008

Lemos JV (2007) Discrete element modeling of masonry structures. Int J Arch Herit 1(2):190–213. http://dx.doi.org/10.1080/15583050601176868

Lourenço PB (1996) Computational strategies for masonry structures. PhD Dissertation. Delft University of Technology

Magenes G, Della Fontana A (1998) Simplified non-linear seismic analysis of masonry buildings. In: 5th international masonry conference. London

Magenes G., Galasco A., Penna A (2009) Caratterizzazione meccanica di una muratura in pietra. In: ANIDIS 2009—XIII convegno di ingegneria sismica in Italia. Bologna, Italy

Milani G, Lourenço PB, Tralli A (2006) Homogenization approach for the limit analysis of out-of-plane loaded masonry walls. Struct Eng 132(10):1650–1663. http://dx.doi.org/10.1061/(ASCE)0733-9445(2006)132:10(1650)

Neves F, Vicente RS, Costa A, Oliveira CS (2008) Seismic vulnerability assessment of the buildings in Faial Island, Azores. International seminar on seismic risk and rehabilitation, Faial, Azores, Portugal

Oliveira CS, Malheiro AM (1999) The Faial, Pico, São Jorge Azores Earthquake of July 9, 1998. LNEC, Lisbon

OPCM no. 3274 (2005) Primi elementi in materiali di criteri generali per la classificazione sismica del territorio nazionale e di normative tecniche per le costruzioni in zona sísmica, come modificato dall'OPCM 3431 del 3/5/05

Page AW (1978) Finite element model for masonry. J Struct Div (ASCE) 104(88):1267–1285

Paulson TJ, Abrams DP (1990) Correlation between static and dynamic response of model masonry structures. Earthq Spectra 6(3):573–592. http://dx.doi.org/10.1193/1.1585587

Penazzi D, Valluzzi MR, Saisi A, Binda L, Modena C (2001) Repair and strengthening of historic masonry buildings in seismic areas. In: Archi 2000. Paris, France, ICOMOS

Pegon P, Pinto AV (1996) Seismic study of monumental structures—structural analysis, modelling and definition of experimental model. JRC, Ispra

Sorrentino L, Kunnath S, Monti G, Scalora G (2008) Seismically induced one-sided rocking response of unreinforced masonry façades. Eng Struct 30:2140–2153. http://dx.doi.org/10.1016/j.engstruct.2007.02.021

Valluzzi MR, da Porto F, Modena C (2001) Behaviour of multi-leaf stone masonry walls strengthened by different intervention techniques. In: Structural analysis of historical constructions. Guimarães, Portugal